

ORIGINAL ARTICLE

Stefin B deficiency reduces tumor growth via sensitization of tumor cells to oxidative stress in a breast cancer model

M Butinar^{1,2}, MT Prebanda¹, J Rajković^{1,2}, B Jerič^{1,2}, V Stoka^{1,2}, C Peters³, T Reinheckel³, A Krüger⁴, V Turk^{1,2,5}, B Turk^{1,5,6} and O Vasiljeva^{1,2,7}

Lysosomal cysteine cathepsins contribute to proteolytic events promoting tumor growth and metastasis. Their enzymatic activity, however, is tightly regulated by endogenous inhibitors. To investigate the role of cathepsin inhibitor stefin B (Stfb) in mammary cancer, *Stfb null* mice were crossed with transgenic polyoma virus middle T oncogene (PyMT) breast cancer mice. We show that ablation of *Stfb* resulted in reduced size of mammary tumors but did not affect their rate of metastasis. Importantly, decrease in tumor growth was correlated with an increased incidence of dead cell islands detected in tumors of *Stfb*-deficient mice. *Ex vivo* analysis of primary PyMT tumor cells revealed no significant effects of ablation of *Stfb* expression on proliferation, angiogenesis, migration and spontaneous cell death as compared with control cells. However, upon treatment with the lysosomotropic agent Leu-Leu-OMe, cancer cells lacking *Stfb* exhibited a significantly higher sensitivity to apoptosis. Moreover, *Stfb*-ablated tumor cells were significantly more prone to cell death under increased oxidative stress. These results indicate an *in vivo* role for *Stfb* in protecting cancer cells by promoting their resistance to oxidative stress and to apoptosis induced through the lysosomal pathway.

Oncogene advance online publication, 19 August 2013; doi:10.1038/onc.2013.314

Keywords: cathepsin inhibitor; stefin; breast cancer; mouse model; oxidative stress

INTRODUCTION

Proteolysis has a crucial role in tumor invasion and metastasis. The roles of lysosomal cysteine proteinases, the cysteine cathepsins, in these processes have been confirmed by numerous clinical reports and evidence accumulated from experimental cancer models.^{1–4} Cathepsins belong to the family of papain-like proteases (clan CA, family C1) and are localized primarily in endosomal and lysosomal compartments.^{5,6} However, under several pathological conditions, these enzymes can escape from endosomal vesicles by being secreted to the extracellular milieu or, alternatively, translocated into the cytosol.⁷ Cysteine cathepsins have been shown to have a clear role as tumor-promoting enzymes,^{8–10} suggesting the possibility of anti-cathepsin therapy in cancer treatment.^{11–15} On the other hand, cysteine cathepsins could participate in induction of tumor cell death through mediation of apoptosis,^{16,17} which, however, requires cytosolic release of these enzymes from lysosomes.¹⁸ An additional level of complexity is introduced by the fact that the proteolytic activity of cysteine cathepsins is regulated by their endogenous inhibitors called cystatins.¹⁹

The endogenous protein inhibitors of cysteine cathepsins, the cystatin superfamily, can be subdivided into three families, stefins (type I), cystatins (type II) and kininogens (type III).²⁰ In mammals, including human, rat, bovine, mouse and porcine, two members of the type I family, stefin A (cystatin A or α) and stefin B (Stfb; cystatin B or β), have been identified. Both inhibitors are single-chain polypeptides with ~100 amino acid residues (molecular mass, ~11 kDa) and are localized intracellularly.²¹ In contrast to

stefin A, which exhibits a restricted expression pattern with especially high levels in skin and some types of blood cells, Stfb is widely distributed in various cell types and tissues. Stfb is considered as a general cytosolic cysteine cathepsin inhibitor in mammalian cells, where it probably serves to protect the cell against inappropriate proteolysis due to cysteine cathepsin leakage from the lysosomes.²² Moreover, it is one of the cystatins for which genetic evidence points to an important biological function. Loss-of-function alterations in the *Stfb* gene (either through a multiplied repeat unit in the promoter region or through point mutations in the structural gene) are present in both alleles of the gene in patients with a form of progressive myoclonus epilepsy.²³ Furthermore, because of the important role of cysteine cathepsins in cancer progression, the ratio of cystatins to cysteine cathepsins has been thoroughly investigated. As such, Stfb levels were correlated with diagnosis and prognosis for cancer patients with different malignancies.²⁴ Strikingly, increased concentrations of Stfb in the body fluids of carcinoma patients have been shown to correlate significantly with shorter survival.²⁵ Although a higher level of cathepsin inhibitors may counterbalance the upregulation of cysteine cathepsins, their role in cancer still remains poorly defined.

To elucidate the role of Stfb (also known as cystatin B) in cancer progression and metastasis, we have established a *Stfb*-ablated mouse mammary cancer model by crossing *Stfb*-deficient mice²⁶ with a strain of mice susceptible to mammary cancer (polyoma virus middle T oncogene (PyMT) mice), which express the PyMT under control of the mouse mammary tumor virus (MMTV) long-

¹Department of Biochemistry and Molecular and Structural Biology, Jožef Stefan Institute, Ljubljana, Slovenia; ²Jožef Stefan International Postgraduate School, Ljubljana, Slovenia;

³Institute of Molecular Medicine and Cell Research, BIOS Centre for Biological Signalling Studies, Albert-Ludwigs-University Freiburg, Freiburg, Germany; ⁴Institut für Experimentelle Onkologie und Therapieforschung des Klinikums rechts der Isar, Technische Universität München, München, Germany; ⁵Centre of Excellence for Integrated Approaches in Chemistry and Biology of Proteins, Ljubljana, Slovenia and ⁶Faculty of Chemistry and Chemical Technology, University of Ljubljana, Ljubljana, Slovenia. Correspondence: Dr O Vasiljeva, The Department of Biochemistry and Molecular and Structural Biology, Jožef Stefan Institute, Jamova 39, Ljubljana 1000, Slovenia. E-mail: olga.vasiljeva@ijs.si

⁷Current address: CytomX Therapeutics Inc., 650 Gateway Boulevard Suite 125, South San Francisco, CA 94080, USA.

Received 17 January 2013; revised 19 May 2013; accepted 17 June 2013

terminal repeat promoter.²⁷ Depletion of *Stfb* has been shown to result in reduced tumor growth, suggesting a novel function for *Stfb* in defending tumor cells against oxidative stress.

RESULTS

Progression of PyMT-induced mammary carcinomas

To examine the role of *Stfb* in the progression of PyMT-induced breast cancer, *Stfb*-deficient mice (*Stfb*^{-/-}) were backcrossed to the FVB/N genetic background for 10 generations. These mice did not show an abnormal behavioral or neurological phenotype at 14 weeks of age, similarly to original *Stfb*^{-/-} inbred C57BL/6 strain.²⁶ These mice were further crossed with PyMT transgenic mice,²⁷ resulting in two groups of female mice, hemizygous for the PyMT transgene: *PyMT;Stfb*^{+/+} and *PyMT;Stfb*^{-/-}. Western blot analyses of *Stfb* revealed overexpression of this inhibitor in mammary tumors of PyMT transgenic mice, relative to the non-transformed mammary glands (Figure 1a). Furthermore, immunohistochemical staining of primary PyMT tumors revealed that *Stfb* was predominantly localized in the tumor cells of *PyMT;Stfb*^{+/+}

tumors and not in the cells of tumor stroma (Figure 1b). To investigate the effect of *Stfb* deficiency in the context of breast cancer, we have compared *PyMT;Stfb*^{+/+} and *PyMT;Stfb*^{-/-} transgenic mice for tumor development, progression, proliferation and cell death. To assess the development of mammary tumors in both groups of mice, all 10 mammary glands of each mouse were palpated three times a week, starting on day 30 after birth in a genotype-blind fashion. To evaluate the genotype-dependent differences in the occurrence of the first palpable tumors, we determined the time point at which cancer-prone mice developed the first two tumors. In the *PyMT;Stfb*^{-/-} group, the first two palpable mammary tumors were detected in all mice at the age of 59 days, which is 6 and 3 days later than in the control *PyMT;Stfb*^{+/+} mice (Figure 1c). Despite the apparent shift of Kaplan–Meier plots for tumor-free mice between the two *Stfb* genotypes, no significant difference between these groups was detected. This data excludes major effects of *Stfb* in initiation of tumor in PyMT mammary cancer model induced by expression of the PyMT transgene. To analyze the effect of *Stfb* on the progression of established tumors, their diameter was measured 30 days after detection. Tumors were grouped by size into the

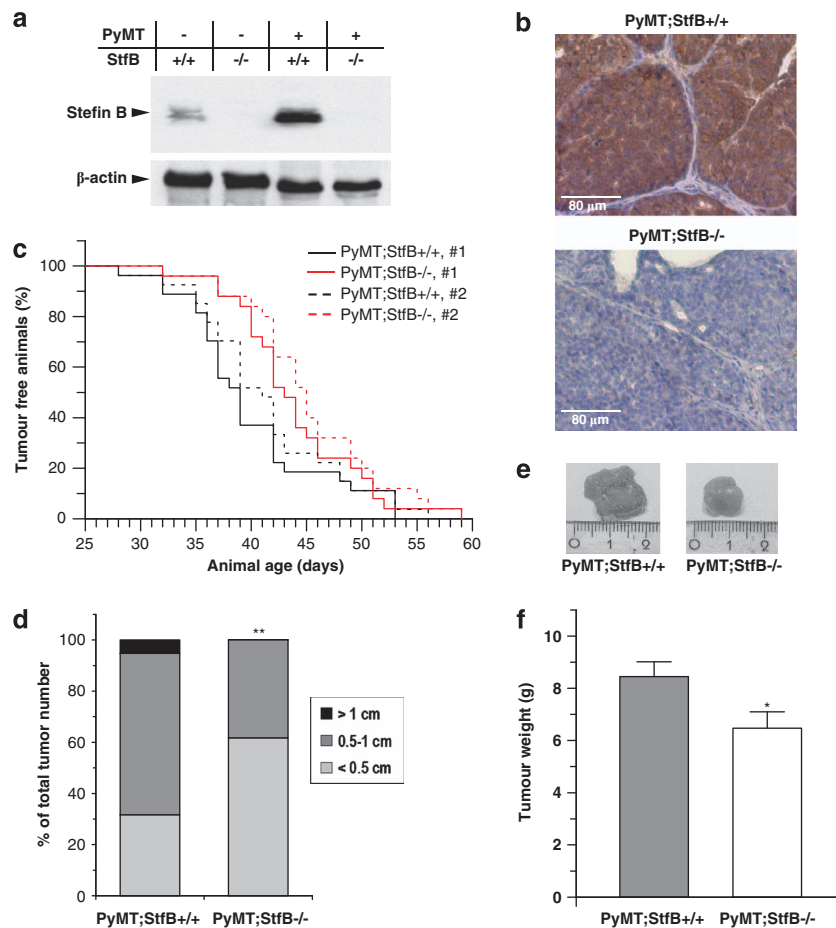


Figure 1. Suppression of PyMT-induced tumor growth in *Stfb*-deficient female mice. **(a)** Expression pattern of *Stfb* in mammary glands and PyMT-induced mammary carcinomas indicates a strong upregulation of *Stfb* in tumor tissue. Western blot analysis of *Stfb*^{+/+}, *Stfb*^{-/-}, *PyMT;Stfb*^{+/+} and *PyMT;Stfb*^{-/-} lysates are shown. β -actin served as a loading control. **(b)** Detection of *Stfb* by immunohistochemistry staining of *PyMT;Stfb*^{+/+} and *PyMT;Stfb*^{-/-} tumor sections. Scale bar, 80 μ m. **(c)** Kaplan–Meier plots for tumor-free *PyMT;Stfb*^{+/+} ($n = 27$) and *PyMT;Stfb*^{-/-} ($n = 25$) female mice. First (no. 1) and second (no. 2) palpable mammary tumors were detected 6 and 3 days later in *PyMT;Stfb*^{-/-} female mice as compared with *PyMT;Stfb*^{+/+} female mice. Statistics were analyzed using log-rank test. **(d)** Size of mammary cancer nodes 30 days after first detection of the individual tumor node. The first 2–3 mammary tumors in each female mouse were analyzed in the *PyMT;Stfb*^{+/+} ($n = 38$) and *PyMT;Stfb*^{-/-} ($n = 47$) cohorts of mice. Proportions were compared statistically by χ^2 -test. $**P < 0.01$. **(e)** Representative images of the single tumors excised from *PyMT;Stfb*^{+/+} and *PyMT;Stfb*^{-/-} mice at 14 weeks of age. **(f)** The cumulative tumor weight per mouse for all mammary tumors was calculated for *PyMT;Stfb*^{-/-} ($n = 23$) and *PyMT;Stfb*^{+/+} ($n = 35$) mice at 14 weeks of age. Statistics were analyzed using Student's t -test. $*P < 0.05$.

three categories based on their diameters: small (<0.5 cm), medium (0.5–1 cm) and large (>1 cm) (Figure 1d). The proportion of those groups was compared between control *PyMT;Stfb*^{+/+} and *PyMT;Stfb*^{-/-} mice revealing significantly lower tumor burden in *PyMT;Stfb*^{-/-} mice. Notably, although 70% of tumors in *PyMT;Stfb*^{+/+} were larger >0.5 cm, only 40% of tumors in *PyMT;Stfb*^{-/-} group were in the range of 0.5–1 cm, and no tumors >1 cm in diameter were detected. At 14 weeks of age, mice were killed and mammary tumors were excised. The finding of the reduced tumor size in *PyMT;Stfb*^{-/-} mice was confirmed *ex vivo* (Figure 1e) and substantiated by the measure of a significant reduction of the cumulative weight of all tumors per mouse in *PyMT;Stfb*^{-/-} cohort of mice, as compared with control *PyMT;Stfb*^{+/+} mice (Figure 1f). Tumors in *Stfb*-deficient mice, with an average weight of 6.47 g, were 23% lighter than those in *PyMT;Stfb*^{+/+} mice, with an average weight of 8.44 g. These results provide evidence for decreased tumor growth associated with depletion of *Stfb* in the breast cancer model.

Effect of *Stfb* ablation on proliferation, cell death and angiogenesis of PyMT-induced mammary carcinomas

Given the substantial differences in growth of PyMT-induced tumors between *PyMT;Stfb*^{-/-} and *PyMT;Stfb*^{+/+} mice, we examined the effect of *Stfb* on hallmark processes of malignant growth, such as tumor proliferation, cell death and angiogenesis, in late-stage primary PyMT tumors. Cell proliferation in mammary tumors was quantified by immunohistochemical detection of the proliferation marker Ki67 (Figure 2a). The numbers of Ki67-positive cells did not differ significantly between tumors with different *Stfb* genotypes (Figure 2b). However, as *Stfb* is localized in the cytosol, its involvement in cell death-related processes could account for the smaller cancers in *PyMT;Stfb*^{-/-} mice. The incidence of dead cells in primary PyMT tumors was determined by terminal dUTP nick-end labeling staining as a measure of DNA fragmentation associated with cell death. Large areas of dead cells were observed in *PyMT;Stfb*^{-/-} mice, unlike in the control group ($P < 0.05$) (Figure 2c). Necrotic areas in tumor samples were measured by computer-assisted histomorphometry. Although areas of dead cells comprised <1.5% of wild-type tumors, these areas comprised 7–8% of examined tumor tissue sections from *PyMT;Stfb*^{-/-} mice (Figure 2d). This observation suggests a role for *Stfb* in tumor cell apoptosis *in vivo*, which was confirmed by immunohistochemical staining for active caspase-3 (Figure 2e and f). To investigate whether this process could be correlated with limited supply of tumors with oxygen and nutrients due to impaired vasculature formation in the growing tumors, we have assessed the effect of *Stfb* on tumor angiogenesis by immunofluorescence staining of the marker CD31. Ablation of *Stfb* had no significant effect on the vessel density in PyMT tumors (Figure 2g). Taken together, these data indicate a specific role for *Stfb* in regulating cell death events in mammary cancer and provide an explanation for the significant reduction of PyMT tumors in *Stfb*-deficient mice.

PyMT tumor cell analysis

To address the role of *Stfb* in tumor cell proliferation and cell death, we examined primary PyMT cells prepared from 14-week-old *PyMT;Stfb*^{+/+} and *PyMT;Stfb*^{-/-} mice. No effect of the *Stfb* genotype on proliferation of primary tumor cells was detected *in vitro* by use of the BrdU assay (Supplementary Figure S1), corroborating the data on Ki67 immunohistochemistry analysis of the tumor tissue. Interestingly, no difference in cell death ratio was detected by measuring the viability of the tumor cells obtained from tumor cells of the two *Stfb* genotypes. However, given the predominant localization of *Stfb* in cytosolic cell compartment, where the lysosomal protease pathway of induction of apoptosis takes place,²⁸ we decided to investigate the role of *Stfb* in

sensitivity of tumor cells to apoptosis induction. Initially, we have measured expression and activity of cysteine cathepsins in tumor lysates of *PyMT;Stfb*^{+/+} and *PyMT;Stfb*^{-/-} mice. Notably, although no difference in expression of cysteine cathepsins was determined by quantitative real-time PCR (Figure 3a), almost a two-fold increase in cathepsin activity was detected in *PyMT;Stfb*^{-/-} tumors (Figure 3b), indicating an important role of this inhibitor in regulation of cathepsins activity. To induce the lysosomal pathway of apoptosis, destabilization of lysosomal membranes in tumor cells of both *Stfb* genotypes was stimulated by the lysosomotropic detergent Leu-Leu-OME. Treatment of cells with Leu-Leu-OME is known to induce cysteine cathepsin leakage into the cytosol, where they degrade the antiapoptotic Bcl-2 family members Bcl-2, Bcl-xL and Mcl-1, and process another Bcl-2 family member Bid into its pro-apoptotic form tBid,^{16,17} leading to activation of the intrinsic apoptosis pathway and activation of caspases 3 and 7. *Stfb*-ablated primary tumor cells were significantly more sensitive to this apoptotic stimulus, resulting in an up to 85% increase in cell death in *PyMT;Stfb*^{-/-} cells, as compared with the 30% of apoptotic cells in *PyMT;Stfb*^{+/+} tumor cells at 1 mM Leu-Leu-OME concentration (Figure 3c). This sensitivity of *Stfb*-depleted tumor cells to a cell death stimulus suggests a possible role of this inhibitor as a 'cell guard' against apoptosis induced by cathepsins. This hypothesis was confirmed by the use of the synthetic cysteine cathepsin inhibitor E64d, which almost completely protected tumor cells from apoptosis (Figure 3c), resulting in an almost fourfold reduction of the number of apoptotic cells. We next measured DEVDase activity of tumor cells after treatment with Leu-Leu-OME, and found it to be threefold higher in *Stfb*-depleted tumor cells (Figure 3d), supporting the above idea. However, upon induction of apoptosis with an anti-CD95 (Fas/APO-1) monoclonal antibody, no significant difference was detected between *PyMT;Stfb*^{+/+} and *PyMT;Stfb*^{-/-} tumor cells as reflected by the number of annexin V-positive cells (Figure 3e). This supports the previous findings that cathepsin release from lysosomes is not a major event in Fas-induced apoptosis,²⁹ thereby providing evidence that the increased level of cell death in *Stfb*-deficient tumors could not be induced by the Fas/CD95 signaling pathway.

Oxidative stress was recently identified as one of the pivotal factors provoking cell death in *Stfb*-ablated neurons, which leads to progressive myoclonus epilepsy disorder.³⁰ Because malignant cells in general are under intrinsic oxidative stress, and are thus more vulnerable to damage by reactive oxygen species (ROS)-generating agents,³¹ we have investigated the effect of *Stfb* deficiency on the sensitivity of tumor cells to induced oxidative stress. Primary tumor cells of both *Stfb* genotypes, *PyMT;Stfb*^{+/+} and *PyMT;Stfb*^{-/-}, were exposed to hydrogen peroxide (H₂O₂), a representative ROS, and tumor cell death was assessed by annexin V staining (Figure 4a). Notably, a significant increase in the percentage of annexin V-positive cells was detected in *PyMT;Stfb*^{-/-} primary tumor cells, as compared with wild-type *PyMT;Stfb*^{+/+} cells (Figure 4b). Moreover, a fivefold increase of DEVDase activity was determined in *PyMT;Stfb*^{-/-} primary tumor cells upon exposure to 1 mM H₂O₂, whereas no difference in caspase activity was detected in wild-type *PyMT;Stfb*^{+/+} cells (Figure 4c). This data indicates an increased sensitivity of *Stfb*-depleted cells to oxidative stress, through induction of apoptotic cell death.

The lack of blood supply in the fast-growing tumors leads to deprivation of nutrients and growth factors that causes increased levels of intracellular ROS.³² Thereby, we have cultured *PyMT;Stfb*^{+/+} and *PyMT;Stfb*^{-/-} cells in serum-free medium (also known as serum starvation) to mimic tumor cell oxidative stress in cell culture. Notably, an increase in tumor cell death was detected in *PyMT;Stfb*^{-/-} tumor cells as compared with *PyMT;Stfb*^{+/+} tumor cells (Supplementary Figure S2). Taken together, our results support the role of *Stfb* as an oxidative

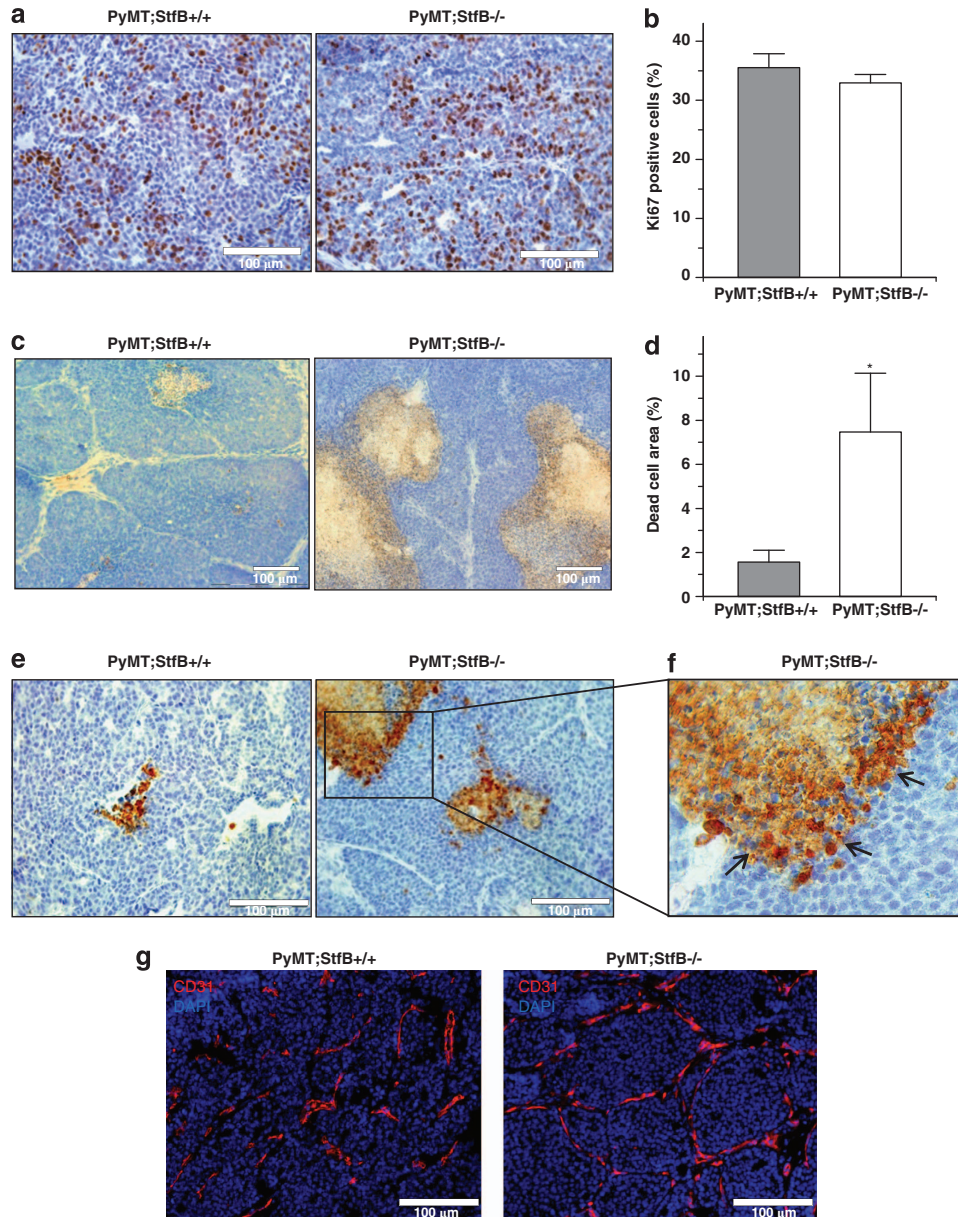


Figure 2. Proliferation, cell death and vessel density in late-stage mammary carcinomas. **(a)** Cell proliferation in primary tumors determined by immunodetection of Ki67 in *PyMT;Stfb*^{+/+} and *PyMT;Stfb*^{-/-} mice at 14 weeks of age. Representative images for each genotype are shown under $\times 40$ magnification. **(b)** Quantification of Ki67-positive cells as percentage of total cells in *PyMT;Stfb*^{+/+} ($n = 13$) and *PyMT;Stfb*^{-/-} ($n = 14$) tumors. Ki67 index was calculated from 20 high-power fields per animal by computer-assisted data analysis using the HistoQuest software (TissueGnostics). **(c)** Immunohistochemical detection of areas of dead cells in primary tumors of *PyMT;Stfb*^{+/+} and *PyMT;Stfb*^{-/-} mice at 14 weeks of age by terminal dUTP nick-end labeling staining. Representative images for each genotype are shown under $\times 40$ magnification. **(d)** The percentage of areas of dead cells was determined on high-power fields of *PyMT;Stfb*^{+/+} ($n = 13$) and *PyMT;Stfb*^{-/-} ($n = 12$) mice tumors by computer-assisted data analysis. Statistics were analyzed using Student's *t*-test. * $P < 0.05$. **(e)** Representative pictures of cell death areas in primary tumors by immunodetection of active caspase-3 in *PyMT;Stfb*^{+/+} and *PyMT;Stfb*^{-/-} mice at 14 weeks of age. Scale bar, 100 μm . **(f)** Higher-magnification image of the selected area of **e** illustrating the specific caspase-3-positive staining in *PyMT;Stfb*^{-/-} mice. **(g)** Representative images of immunofluorescence staining of the endothelial cell-specific marker CD31 (red staining) on *PyMT;Stfb*^{+/+} and *PyMT;Stfb*^{-/-} tumors.

stress-resistance factor, limiting the sensitivity of a tumor cell to hypoxia and nutrient restriction.

DISCUSSION

Cysteine cathepsins have a dual role in cancer progression. First, they promote tumor invasion through (i) activation of the extracellular proteolytic cascade(s), (ii) degradation of the extracellular matrix and (iii) inactivation of adhesion molecules, for

example, E-cadherin. Second, they participate in the apoptotic pathways. Although these two activities have apparently opposing functions, there is a clear physical separation of the processes in different cell compartments, allowing for the possibility of their selective targeting.⁷ Although the proteolysis required for tumor invasion occurs mostly in the extracellular space,^{1,2} the apoptotic pathway is clearly intracellular and dependent on translocation of cathepsins from the endosomal/lysosomal compartment into the cytosol.^{5,18} In the present study, we have investigated the role of

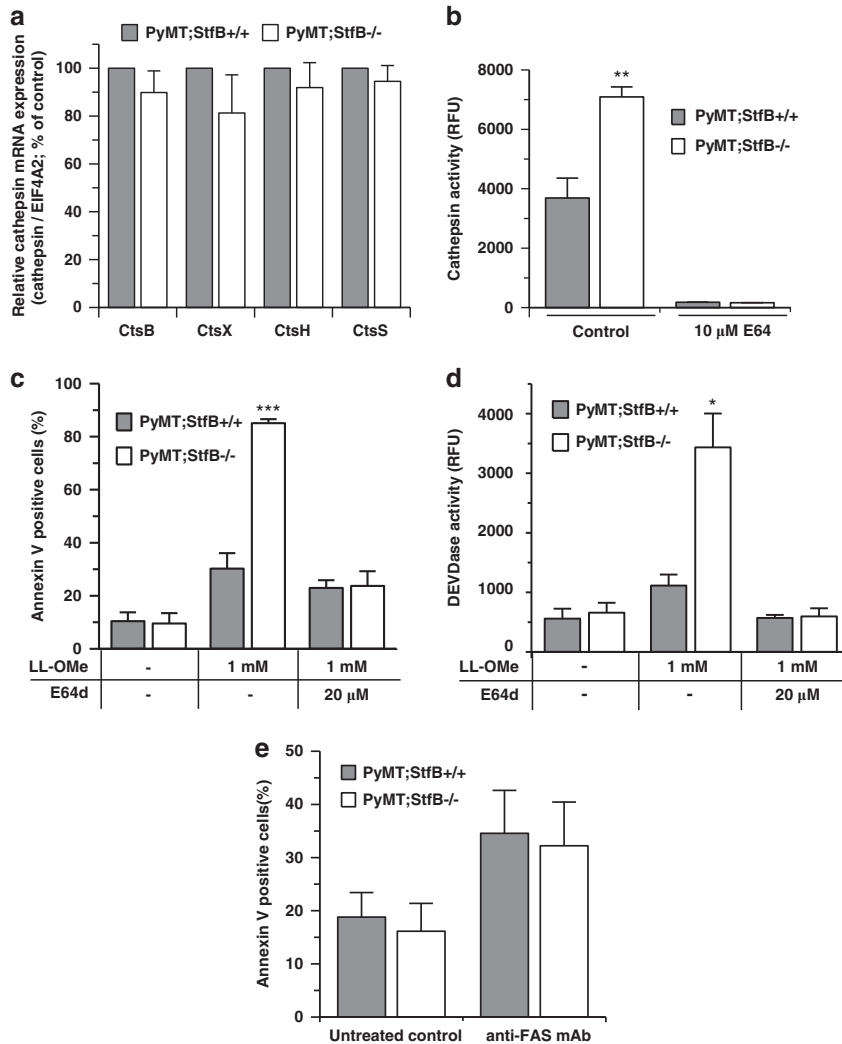


Figure 3. Ablation of *Stfb* leads to increased sensitivity of primary *PyMT* tumor cells to apoptosis induced with lysosomotropic agent. **(a)** Expression of cysteine cathepsins in *PyMT;Stfb*^{+/+} (*n* = 4) and *PyMT;Stfb*^{-/-} (*n* = 4) primary mammary tumors. Comparison of mRNA expression of cathepsin B (Ctsb), cathepsin X (Ctsx), cathepsin H (Ctsh) and cathepsin S (Ctss) in tumor samples was measured by quantitative real-time PCR. Data are presented as means and s.e., expressed as a percentage of the control (100%). **(b)** Activity of cysteine cathepsins in tumor tissue determined by hydrolysis of fluorogenic substrate Z-Phe-Arg-AMC on *PyMT;Stfb*^{+/+} (*n* = 5) and *PyMT;Stfb*^{-/-} (*n* = 6) mammary tumor lysates in the presence or absence of E64 inhibitor. Data are presented as means and s.e. Statistics were analyzed using Student's *t*-test. **(c)** Leu-Leu-OMe (LL-OMe) concentration-dependent cell death in *PyMT;Stfb*^{+/+} (*n* = 4) and *PyMT;Stfb*^{-/-} (*n* = 4) primary tumor cells. Cell death was measured by fluorescence-activated cell sorting analysis using annexin V-phycoerythrin. **(d)** DEVDase activity in Leu-Leu-OMe-treated *PyMT;Stfb*^{+/+} (*n* = 4) and *PyMT;Stfb*^{-/-} (*n* = 4) primary tumor cells. Data are presented as means and s.e. Statistics were analyzed using Student's *t*-test. **(e)** Fas dose-dependent cell death in *PyMT;Stfb*^{+/+} (*n* = 4) and *PyMT;Stfb*^{-/-} (*n* = 4) primary tumor cells was assessed after 18 h of stimulation in the presence of CHX (1 μg/ml).

the intracellular inhibitor of cysteine cathepsins, *Stfb*, which is localized predominantly in the cytosol,²² where it serves to protect the cell against leakage of lysosomal enzymes. Consistent with that, depletion of *Stfb* had no effect on tumor invasion and metastasis-related processes (data not shown) that require translocation of cysteine cathepsins to the extracellular milieu. In contrast, significant reduction of tumor size and weight was observed in the *PyMT;Stfb*^{-/-} group of mice, which correlated with the increased level of tumor cell death in tumors depleted of *Stfb* (Figure 2c–f). Surprisingly, given the well-substantiated role of cysteine cathepsins in various cell death pathways, no difference in spontaneous levels of apoptosis was detected between *PyMT;Stfb*^{+/+} and *PyMT;Stfb*^{-/-} primary tumor cells. However, according to current knowledge, cysteine cathepsins must be released into the cytosol in order to be involved in propagation of apoptosis.³³ To enable this, lysosomal membrane

destabilization is required, which could be triggered by different lysosomotropic compounds, such as detergents, including the amino acid methyl ester Leu-Leu-OMe,^{16,17,34,35} which are able to induce lysosomal membrane permeabilization. In agreement with that, a significant increase in apoptosis was observed in *Stfb*-depleted primary *PyMT* tumor cells as compared with the wild-type tumor cells (Figure 3c and d). Moreover, this result is consistent with the previous report on depletion of cysteine cathepsin B in the same tumor model, where primary tumor cells were significantly less sensitive to apoptosis induced by Leu-Leu-OMe.³⁶

Furthermore, lysosomal membranes can be destabilized by low concentrations of H₂O₂,^{37–40} which is a physiological mediator of cell death. Growing evidence suggests that cancer cells produce high levels of ROS and are constantly under oxidative stress.^{31,41–43} Moreover, it is generally accepted that oxidative stress has an

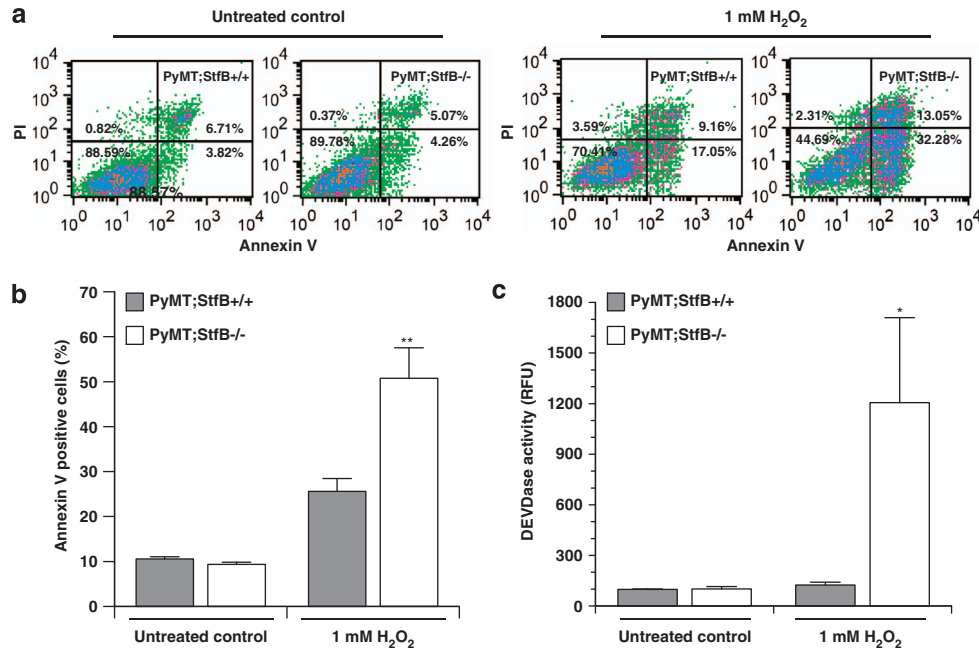


Figure 4. Stfb is associated with resistance of PyMT tumor cells to oxidative stress. **(a)** Fluorescence-activated cell sorting analysis of annexin V–phycoerythrin and propidium iodide (PI)-stained *PyMT;Stfb*^{+/+} (*n* = 6) and *PyMT;Stfb*^{-/-} (*n* = 6) primary tumor cells. Left two columns: untreated controls; right two columns: after treatment with 1 mM H₂O₂ for 18 h. **(b)** Ablation of Stfb leads to increase of H₂O₂-induced programmed cell death in PyMT tumor cells determined as a percentage of annexin V-positive cells after treatment with 1 mM H₂O₂ for 18 h. Data are presented as means and s.e. ***P* < 0.01. **(c)** DEVDase activity determined in the cell extracts of 1 mM H₂O₂-treated *PyMT;Stfb*^{+/+} and *PyMT;Stfb*^{-/-} primary tumor cells. Data are presented as means and s.e. Statistics were analyzed using Student's *t*-test. **P* < 0.05.

important role in apoptosis in carcinomas. H₂O₂ is a ubiquitous ROS that is generated from nearly all sources of oxidative stress and can freely cross cell membranes. It has been widely used to model ROS-induced apoptosis in experimental situations.^{44–46} Recently, H₂O₂-dependent lysosomal destabilization has been described in human prostate cancer PC-3 cells⁴⁷ and in human leukemia HL-60 cells.³⁸ Moreover, an involvement of lysosomal cysteine proteinases has been confirmed in the latter study by the use of E64d inhibitor. These data propose that in the absence of Stfb the protection of cells against ROS-induced apoptosis could be reduced. This hypothesis is supported by the results of Lehtinen *et al.*,³⁰ who have shown that knocking out Stfb or reducing its levels sensitizes cerebellar granule neurons to oxidative stress-induced cell death, resulting in neuronal death and degeneration.³⁰ This explains why the absence of this inhibitor triggers progressive degeneration of cerebellar granule neurons, leading to progressive myoclonus epilepsy (EPM1).²³ In our study, we have clearly demonstrated an increased sensitivity of breast tumor cells lacking Stfb to H₂O₂ and serum starvation-induced apoptosis compared with the wild-type tumor cells (Figure 4 and Supplementary Figure S2). This not only is in agreement with previous findings on cerebellar granule neurons but also suggests a novel function for Stfb in defending tumor cells from oxidative stress. Moreover, the recent findings on sensitization of thymocytes to staurosporin-induced apoptosis⁴⁸ and melanoma cells to tumor necrosis factor-related apoptosis-inducing ligand-induced apoptosis,⁴⁹ upon gene knockout or short hairpin RNA knockdown of Stfb, respectively, support the protective function of Stfb against apoptosis. Interestingly, a role of Stfb in stabilization of the FADD like IL beta converting enzyme (FLICE)-like inhibitory protein, which can interrupt apoptotic signaling at the death-inducing signaling complex (DISC) level by competing with caspase-8 for binding to Fas Associated protein with death domain (FADD), was recently discovered on melanoma cell lines,⁴⁹ thus proposing a cathepsin activity-independent function for Stfb. Furthermore, the results on the

tumor-protective role of Stfb may explain the clinical data showing that higher levels of Stfb in tumor tissues and body fluids are associated with poor prognosis for patients with different types of cancer. These reports are also supported by the recent data on a proteome analysis of differentially expressed proteins by mass spectrometry, where Stfb was identified as a tissue and urinary biomarker of bladder cancer recurrence and progression.⁵⁰ Moreover, elevated Stfb level was also determined as the most significant variable predicting disease recurrence and grade/stage progression of transitional cell carcinoma.⁵⁰

Interestingly, depletion of extracellular cysteine cathepsin inhibitor, cystatin C, results in a reduction of epithelial cell apoptosis and increase of proliferation and angiogenesis in a mouse model of multistage epithelial carcinogenesis.⁵¹ Thus, collectively, the results of Yu *et al.*⁵¹ and our data provide additional evidence for the importance of the subcellular localization of the disrupted protease–protease inhibitor counterbalance for the impact on tumor progression: extracellular for cystatin C and cytosolic for Stfb. Moreover, the data for another intracellular inhibitor of cysteine cathepsins, stefin A, corroborate this hypothesis revealing the association of stefin A expression with poor histological differentiation, high proliferative activity and increased risk of death in tumors of breast cancer patients.⁵² Furthermore, similarly to our Stfb model, tumors positive for stefin A were larger than stefin A-negative tumors.⁵²

Carcinoma cells synthesize ROS at a high rate, and many tumors thus appear to be under persistent oxidative stress.⁴¹ However, many cancer cells become well adapted to such stress and develop resistance to oxidative stress and ROS-mediated apoptosis. Our results suggest an important role of Stfb for building up such resistance by protecting cells against apoptosis, thereby promoting tumor cell survival and cancer progression. This underlines the need for further research of the molecular signaling pathways regulated by the protease inhibitors⁵³ and the development of new strategies for cancer therapy to enhance therapeutic activity and selectivity.

MATERIALS AND METHODS

Animals

Mice were used in accordance with protocols approved by the Veterinary Administration of the Republic of Slovenia and the government Ethical Committee. Procedures for animal care and use were in accordance with the 'PHS Policy on Human Care and Use of Laboratory Animals' and the 'Guide for the Care and Use of Laboratory Animals'. The *Stfb*-deficient mouse strain was kindly provided by Dr Richard M. Myers.²⁶ *Stfb*^{-/-} mice were backcrossed for eight generations to the transgenic mouse strain expressing PyMT under the control of MMTV long-terminal repeat promoter (FVB/N-TgN (MMTVpyVT)634-Mul).²⁷ After the intercross, wild-type and *Stfb*-deficient tumor bearing mice were named *PyMT;Stfb*^{+/+} and *PyMT;Stfb*^{-/-}, respectively. Animals were bred and maintained in accordance with the Slovenian law for animal protection.

Tumor progression study

Beginning at age 30 days, female mice were examined three times a week for the development of mammary tumors by finger palpation in a genotype-blinded fashion. Their diameters were measured 30 days after being first detected. At the age of 14 weeks, mice were killed and all 10 mammary tumors were excised and weighed.

Histomorphometry

For volumetric measurement of total lung metastasis or disseminated tumor colonies in lungs, the paraffin-embedded lungs were cut into 5- μ m thick slices from at least three different planes. Each section was stained with hematoxylin and eosin. The average metastasis size was determined by computer-assisted measurement using Cellquest software (Olympus, Tokyo, Japan).

Immunohistochemistry and immunofluorescence

Histological measurement of proliferation by Ki67 staining, cell death and tumor vascularization rate by CD31 staining were done as described.^{9,36} Right (thoracic) mammary glands were sectioned, and tissue sections for each tumor were taken from *PyMT;Stfb*^{+/+} and *PyMT;Stfb*^{-/-} mice. Rabbit anti-active caspase-3 antibody (Abcam ab2302, Cambridge, UK; 1:40 dilution) was used to detect apoptotic epithelial and cancer cells. Rabbit anti-mouse *Stfb* antibodies (Abcam, Cambridge, UK, ab53725; 1:1000 dilution) were used for immunohistochemical detection of *Stfb*. Detection of primary antibodies was done by Vectastain Elite ABC kit (Vector Laboratories, Burlingame, CA, USA) in accordance to the manufacturer's instructions, followed by incubation with 3,3-DAB (Sigma-Aldrich, Steinheim, Germany) and nuclear staining with hematoxylin. For Ki67 data assessment, 20 fields per tumor were selected at random, using a \times 40 objective, and quantified using TissueQuest software (TissueGnostics, Vienna, Austria). Areas of dead cells in tumor sections were determined using the ApoptTag Peroxidase In Situ apoptosis detection Kit (Millipore, Billerica, MA, USA) and an Olympus microscope (Olympus IX 81) with Imaging Software for Life Science Microscopy Cell. For vascularization, samples were co-stained and mounted in SlowFade Gold antifade reagent with DAPI (Invitrogen) and examined with an Olympus fluorescence microscope (Olympus IX 81) with Imaging Software for Life Science Microscopy Cell.

Isolation of primary tumor cells from PyMT-induced mammary carcinomas

Primary MMTV-PyMT cells were isolated and cultured as described.¹⁰ Only low-passage number cells (<4 passages total) were used for experiments. All primary cells were maintained in DMEM (Gibco, (Invitrogen), Paisley, Scotland, UK) supplemented with 10% fetal bovine serum (Sigma-Aldrich, St Louis, MO, USA), 2 mM L-glutamine (Invitrogen), 100 U of penicillin and 100 μ g/ml streptomycin (Invitrogen). Cultured cells were maintained at 37 °C in a humidified 5% CO₂ atmosphere.

Quantitative real-time PCR

Total RNA was isolated from flash-frozen PyMT mammary tumors with an Allprep DNA/RNA/Protein Mini kit (Qiagen, Valencia, CA, USA) and treated with TURBO DNA-free kit (Ambion, Life Technologies, Foster City, CA, USA) for genomic DNA elimination. RNA quality (A260/230 and A260/280 ratios) was assessed spectrophotometrically, whereas RNA integrity was confirmed by 1.2% gel electrophoresis. RNA was further reverse transcribed into cDNA

with a random nanomer primers using Precision nanoScript Reverse Transcription kit (Primerdesign Ltd, Southampton, UK). mRNA expression levels of cathepsin B, cathepsin S, cathepsin X and cathepsin H were detected by SYBR green detection chemistry using 2 \times Precision MasterMix (Primerdesign Ltd). Eukaryotic translation initiation factor 4A2 was selected as the most stable expressed reference gene by GeNorm reference gene selection kit (Primerdesign Ltd), and normalized values were used to calculate the relative mRNA expression of individual genes. Quantitative real-time PCR reaction was run on Mx3005P Real-time PCR system (Agilent, Stratagene products, Waldbronn, Germany) using the following conditions: 95 °C for 10 min (an initial denaturation step) followed by 40 cycles of 95 °C for 15 s and 60 °C for 1 min (annealing and extension). In addition, melting curve (55–95 °C) was performed at the end of each run. Intron spanning gene-specific primers (Primerdesign Ltd) were as follows: cathepsin B, 5'-TACTTGCTGTGGTATCCAGTGTG-3' (forward) and 5'-ATGGTGTATGGTAAGCAGCCTAC-3' (reverse); cathepsin S, 5'-CTGTTCTTGACAAGCCAATTTTATTC-3' (forward) and 5'-AGCCAGTAATCTTGCCATCA-3' (reverse); cathepsin X, 5'-CTATGCCAATGGTCCCATCAG-3' (forward) and 5'-CCTGGTCCTGGTGCTCAG-3' (reverse); and cathepsin H, 5'-TTTGATGTATAAAAGTGGCGTCTA-3' (forward) and 5'-GAGTTTTTCAC AATCCAGTAGAGT-3' (reverse). The relative expression ratios of target genes were calculated considering their real-time PCR efficiencies.

Induction of apoptosis

Apoptosis was induced with anti-CD95 monoclonal antibody Jo-2 (BD Pharmingen, San Diego, CA, USA) at a final concentration of 0.2 μ g/ml in the presence of cyclohexamide (CHX) for 18 h. The mediator of oxidative stress, H₂O₂, was applied at a final concentration of 1 mM for 18 h. The lysosomotropic agent Leu-Leu-OMe was applied at final concentration of 1 mM with or without 20 μ M E64d for 18 h.¹⁶ At indicated time points, cells were harvested and lysed (50 mM HEPES, 200 mM NaCl, 0.1% (w/v) CHAPS, 10% (w/v) sucrose, 5 mM MgCl₂, 0.02 (w/v) BSA, 1% (w/v) NP-40 and 0.5% (w/v) Triton X-100) on ice then centrifuged at 10000 g (10 min), and supernatants were separated. Total protein concentration was determined using the Bradford assay (Bio-Rad, München, Germany). Cells, untreated and treated with anti-CD95 monoclonal antibody, 1 mM H₂O₂ or 1 mM Leu-Leu-OMe, were labeled with annexin V-phycoerythrin/7AAD (BD Pharmingen). Exposure to phosphatidylserine and DNA fragmentation were measured by labeling cells with annexin V-phycoerythrin in the presence of propidium iodide according to the manufacturer's instructions. Cells were then subjected to flow cytometry (fluorescence-activated cell sorting) analysis using FACScalibur flow cytometer (Becton Dickinson, Franklin Lakes, NJ, USA).

Cathepsin activity in mammary tumor lysates

Frozen tissues of primary tumors were disrupted in 200 μ l of 0.1 M TRIS buffer pH 8.5, 5 mM EDTA, 200 mM sodium chloride and 0.2% SDS, using an Ultrathurrax (IKA, Staufen, Germany), and centrifuged at 1000 g for 10 min. Cysteine cathepsin activity was determined by hydrolysis of the general cathepsin substrate Z-Phe-Arg-4-methyl-coumarin-7-amide (Z-Phe-Arg-AMC, 10 μ M; Bachem, Bubendorf, Switzerland) in 0.1 M phosphate buffer, pH 6.0, containing 1 mM EDTA, 0.1% (v/v) polyethylene glycol and 1 mM dithiothreitol, in the presence or absence of E64 cysteine cathepsin inhibitor at a final concentration of 10 μ M. Kinetics of substrate hydrolysis were monitored continuously during 10 min by Tecan Infinite M1000 PRO (Tecan, Gröding, Austria) plate reader at excitation and emission wavelengths of 370 and 460 nm, respectively.

DEVDase activity

Cell lysates (75 μ g of protein) were transferred into a black 96-well plate. Caspase buffer (50 mM HEPES, 200 mM NaCl, 0.1% (w/v) CHAPS, 10% (w/v) sucrose, 5 mM MgCl₂ and 0.02 (w/v) BSA) was added to a final volume of 90 μ l and incubated for 15 min at 37 °C. A volume of 10 μ l acetyl-DEVD-7-amino-4-trifluoromethylcoumarin (Bachem) was added to a final concentration of 100 μ M, and DEVDase activity was measured by Tecan Infinite M1000 PRO (Tecan) plate reader at excitation and emission wavelengths of 400 and 505 nm, respectively.

Immunoblotting

Equal amounts (100 μ g) of protein were resolved on 12.5% SDS polyacrylamide gel electrophoresis gels and electrotransferred to polyvinylidene difluoride membranes. Blots were probed with rabbit anti-*Stfb*

antibodies (Abcam; ab53725, 1:1000 dilution) and rabbit anti-actin antibodies (Sigma-Aldrich) at 1:800 and 1:2000 dilutions, respectively. Secondary conjugated goat anti-rabbit antibodies were used at 1:5000 dilutions.

Statistical analysis

Quantitative data are presented as means \pm s.e. The differences were compared using Student's *t*-test. Proportions were compared using the χ^2 -test, and statistical analysis of Kaplan–Meier plots was done by log-rank test. When *P*-values were ≤ 0.05 , differences were considered statistically significant.

CONFLICT OF INTEREST

The authors declare no conflict of interest.

ACKNOWLEDGEMENTS

We thank Richard Myers and Len Pennacchio, formerly of Stanford University, for providing with Sfbf knockout mouse strain, Georgy Mikhaylov and Matej Vizovisek for their technical and methodological assistance, Eva Zerovnik for valuable discussions and Roger H. Pain for critical reading of the manuscript. This work was supported by the European Commission FP7 grant 201279 (Microenvimet: CP, TR, AK, BT and OV), the Slovenian Research Agency (research grants no. J3-4267 to OV and P1-0140 to BT) and Deutsche Forschungsgemeinschaft SFB 850 project B7 (CP and TR).

REFERENCES

- Gocheva V, Joyce JA. Cysteine cathepsins and the cutting edge of cancer invasion. *Cell Cycle* 2007; **6**: 60–64.
- Mohamed MM, Sloane BF. Cysteine cathepsins: multifunctional enzymes in cancer. *Nat Rev Cancer* 2006; **6**: 764–775.
- Turk V, Kos J, Turk B. Cysteine cathepsins (proteases)—on the main stage of cancer? *Cancer Cell* 2004; **5**: 409–410.
- Vasiljeva O, Reinheckel T, Peters C, Turk D, Turk V, Turk B. Emerging roles of cysteine cathepsins in disease and their potential as drug targets. *Curr Pharm Des* 2007; **13**: 387–403.
- Turk B, Turk V. Lysosomes as 'suicide bags' in cell death: myth or reality? *J Biol Chem* 2009; **284**: 21783–21787.
- Turk V, Stoka V, Vasiljeva O, Renko M, Sun T, Turk B et al. Cysteine cathepsins: from structure, function and regulation to new frontiers. *Biochim Biophys Acta* 2012; **1824**: 68–88.
- Vasiljeva O, Turk B. Dual contrasting roles of cysteine cathepsins in cancer progression: Apoptosis versus tumour invasion. *Biochimie* 2008; **90**: 380–386.
- Gocheva V, Zeng W, Ke D, Klimstra D, Reinheckel T, Peters C et al. Distinct roles for cysteine cathepsin genes in multistage tumorigenesis. *Genes Dev* 2006; **20**: 543–556.
- Sevenich L, Schurigt U, Sachse K, Gajda M, Werner F, Muller S et al. Synergistic antitumor effects of combined cathepsin B and cathepsin Z deficiencies on breast cancer progression and metastasis in mice. *Proc Natl Acad Sci USA* 2010; **107**: 2497–2502.
- Vasiljeva O, Papazoglou A, Kruger A, Brodoefel H, Korovin M, Deussing J et al. Tumor cell-derived and macrophage-derived cathepsin B promotes progression and lung metastasis of mammary cancer. *Cancer Res* 2006; **66**: 5242–5250.
- Bell-McGuinn KM, Garfall AL, Bogoy M, Hanahan D, Joyce JA. Inhibition of cysteine cathepsin protease activity enhances chemotherapy regimens by decreasing tumor growth and invasiveness in a mouse model of multistage cancer. *Cancer Res* 2007; **67**: 7378–7385.
- Gopinathan A, Denicola GM, Frese KK, Cook N, Karreth FA, Mayerle J et al. Cathepsin B promotes the progression of pancreatic ductal adenocarcinoma in mice. *Gut* 2012; **61**: 877–884.
- Joyce JA, Baruch A, Chehade K, Meyer-Morse N, Giraudo E, Tsai FY et al. Cathepsin cysteine proteases are effectors of invasive growth and angiogenesis during multistage tumorigenesis. *Cancer Cell* 2004; **5**: 443–453.
- Mikhaylov G, Mikac U, Magaeva AA, Itin VI, Naiden EP, Psakhie I et al. Ferri-liposomes as an MRI-visible drug-delivery system for targeting tumours and their microenvironment. *Nat Nanotechnol* 2011; **6**: 594–602.
- Shree T, Olson OC, Elie BT, Kester JC, Garfall AL, Simpson K et al. Macrophages and cathepsin proteases blunt chemotherapeutic response in breast cancer. *Genes Dev* 2011; **25**: 2465–2479.
- Cirman T, Oresic K, Mazovec GD, Turk V, Reed JC, Myers RM et al. Selective disruption of lysosomes in HeLa cells triggers apoptosis mediated by cleavage of Bid by multiple papain-like lysosomal cathepsins. *J Biol Chem* 2004; **279**: 3578–3587.
- Droga-Mazovec G, Bojic L, Petelin A, Ivanova S, Romih R, Repnik U et al. Cysteine cathepsins trigger caspase-dependent cell death through cleavage of Bid and antiapoptotic Bcl-2 homologues. *J Biol Chem* 2008; **283**: 19140–19150.
- Stoka V, Turk V, Turk B. Lysosomal cysteine cathepsins: signaling pathways in apoptosis. *Biol Chem* 2007; **388**: 555–560.
- Turk B, Turk D, Salvesen GS. Regulating cysteine protease activity: essential role of protease inhibitors as guardians and regulators. *Curr Pharm Des* 2002; **8**: 1623–1637.
- Turk V, Stoka V, Turk D. Cystatins: biochemical and structural properties, and medical relevance. *Front Biosci* 2008; **13**: 5406–5420.
- Turk B, Turk V, Turk D. Structural and functional aspects of papain-like cysteine proteinases and their protein inhibitors. *Biol Chem* 1997; **378**: 141–150.
- Alakurtti K, Weber E, Rinne R, Theil G, Haan G-Jd, Lindhout D et al. Loss of lysosomal association of cystatin B proteins representing progressive myoclonus epilepsy, EPM1, mutations. *Eur J Hum Genet* 2004; **13**: 208–215.
- Pennacchio LA, Lehesjoki AE, Stone NE, Willour VL, Virtaneva K, Miao J et al. Mutations in the gene encoding cystatin B in progressive myoclonus epilepsy (EPM1). *Science* 1996; **271**: 1731–1734.
- Jedieszko C, Sloane BF. Cysteine cathepsins in human cancer. *Biol Chem* 2004; **385**: 1017–1027.
- Kos J, Krasovec M, Cimerman N, Nielsen HJ, Christensen IJ, Brunner N. Cysteine proteinase inhibitors stefin A, stefin B, and cystatin C in sera from patients with colorectal cancer: relation to prognosis. *Clin Cancer Res* 2000; **6**: 505–511.
- Pennacchio LA, Bouley DM, Higgins KM, Scott MP, Noebels JL, Myers RM. Progressive ataxia, myoclonic epilepsy and cerebellar apoptosis in cystatin B-deficient mice. *Nat Genet* 1998; **20**: 251–258.
- Guy CT, Cardiff RD, Muller WJ. Induction of mammary tumors by expression of polyomavirus middle T oncogene: a transgenic mouse model for metastatic disease. *Mol Cell Biol* 1992; **12**: 954–961.
- Stoka V, Turk B, Schendel SL, Kim TH, Cirman T, Snipas SJ et al. Lysosomal protease pathways to apoptosis. Cleavage of bid, not pro-caspases, is the most likely route. *J Biol Chem* 2001; **276**: 3149–3157.
- Bojic L, Petelin A, Stoka V, Reinheckel T, Peters C, Turk V et al. Cysteine cathepsins are not involved in Fas/CD95 signalling in primary skin fibroblasts. *FEBS Lett* 2007; **581**: 5185–5190.
- Lehtinen MK, Tegelberg S, Schipper H, Su H, Zukor H, Manninen O et al. Cystatin B deficiency sensitizes neurons to oxidative stress in progressive myoclonus epilepsy, EPM1. *J Neurosci* 2009; **29**: 5910–5915.
- Hileman EO, Liu J, Albitar M, Keating MJ, Huang P. Intrinsic oxidative stress in cancer cells: a biochemical basis for therapeutic selectivity. *Cancer Chemother Pharmacol* 2004; **53**: 209–219.
- Rygiel TP, Mertens AE, Strumane K, van der Kammen R, Collard JG. The Rac activator Tiam1 prevents keratinocyte apoptosis by controlling ROS-mediated ERK phosphorylation. *J Cell Sci* 2008; **121**: 1183–1192.
- Repnik U, Turk B. Lysosomal-mitochondrial cross-talk during cell death. *Mitochondrion* 2010; **10**: 662–669.
- Goldman R, Kaplan A. Rupture of rat liver lysosomes mediated by L-amino acid esters. *Biochim Biophys Acta* 1973; **318**: 205–216.
- Uchimoto T, Nohara H, Kamehara R, Iwamura M, Watanabe N, Kobayashi Y. Mechanism of apoptosis induced by a lysosomotropic agent, L-Leucyl-L-Leucine methyl ester. *Apoptosis* 1999; **4**: 357–362.
- Vasiljeva O, Korovin M, Gajda M, Brodoefel H, Bojic L, Krüger A et al. Reduced tumour cell proliferation and delayed development of high-grade mammary carcinomas in cathepsin B-deficient mice. *Oncogene* 2008; **27**: 4191–4199.
- Antunes F, Cadenas E, Brunk UT. Apoptosis induced by exposure to a low steady-state concentration of H₂O₂ is a consequence of lysosomal rupture. *Biochem J* 2001; **356**: 549–555.
- Ishisaka R, Utsumi K, Utsumi T. Involvement of lysosomal cysteine proteases in hydrogen peroxide-induced apoptosis in HL-60 cells. *Biosci Biotechnol Biochem* 2002; **66**: 1865–1872.
- Takahashi T, Kitaoka K, Ogawa Y, Kobayashi T, Seguchi H, Tani T et al. Lysosomal dysfunction on hydrogen peroxide-induced apoptosis of osteoarthritic chondrocytes. *Int J Mol Med* 2004; **14**: 197–200.
- Yin L, Stearns R, Gonzalez-Flecha B. Lysosomal and mitochondrial pathways in H₂O₂-induced apoptosis of alveolar type II cells. *J Cell Biochem* 2005; **94**: 433–445.
- Brown NS, Bicknell R. Hypoxia and oxidative stress in breast cancer. Oxidative stress: its effects on the growth, metastatic potential and response to therapy of breast cancer. *Breast Cancer Res* 2001; **3**: 323–327.
- Szatrowski TP, Nathan CF. Production of large amounts of hydrogen peroxide by human tumor cells. *Cancer Res* 1991; **51**: 794–798.
- Toyokuni S, Okamoto K, Yodoi J, Hiai H. Persistent oxidative stress in cancer. *FEBS Lett* 1995; **358**: 1–3.

- 44 Datta K, Babbar P, Srivastava T, Sinha S, Chattopadhyay P. p53 dependent apoptosis in glioma cell lines in response to hydrogen peroxide induced oxidative stress. *Int J Biochem Cell Biol* 2002; **34**: 148–157.
- 45 Mao Y, Song G, Cai Q, Liu M, Luo H, Shi M *et al*. Hydrogen peroxide-induced apoptosis in human gastric carcinoma MGC803 cells. *Cell Biol Int* 2006; **30**: 332–337.
- 46 Zuliani T, Denis V, Noblesse E, Schnebert S, Andre P, Dumas M *et al*. Hydrogen peroxide-induced cell death in normal human keratinocytes is differentiation dependent. *Free Radic Biol Med* 2005; **38**: 307–316.
- 47 Kariya S, Sawada K, Kobayashi T, Karashima T, Shuin T, Nishioka A *et al*. Combination treatment of hydrogen peroxide and X-rays induces apoptosis in human prostate cancer PC-3 cells. *Int J Radiat Oncol Biol Phys* 2009; **75**: 449–454.
- 48 Kopitar-Jerala N, Schweiger A, Myers RM, Turk V, Turk B. Sensitization of stefin B-deficient thymocytes towards staurosporin-induced apoptosis is independent of cysteine cathepsins. *FEBS Lett* 2005; **579**: 2149–2155.
- 49 Yang F, Tay KH, Dong L, Thorne RF, Jiang CC, Yang E *et al*. Cystatin B inhibition of TRAIL-induced apoptosis is associated with the protection of FLIP(L) from degradation by the E3 ligase itch in human melanoma cells. *Cell Death Differ* 2010; **17**: 1354–1367.
- 50 Feldman AS, Banyard J, Wu CL, McDougal WS, Zetter BR. Cystatin B as a tissue and urinary biomarker of bladder cancer recurrence and disease progression. *Clin Cancer Res* 2009; **15**: 1024–1031.
- 51 Yu W, Liu J, Shi MA, Wang J, Xiang M, Kitamoto S *et al*. Cystatin C deficiency promotes epidermal dysplasia in K14-HPV16 transgenic mice. *PLoS ONE* 2010; **5**: e13973.
- 52 Kuopio T, Kankaanranta A, Jalava P, Kronqvist P, Kotkansalo T, Weber E *et al*. Cysteine proteinase inhibitor cystatin A in breast cancer. *Cancer Res* 1998; **58**: 432–436.
- 53 Turk B, Turk D, Turk V. Protease signalling: the cutting edge. *EMBO J* 2012; **31**: 1630–1643.

Supplementary Information accompanies this paper on the Oncogene website (<http://www.nature.com/onc>)